Materials Research. 2015; 18(Suppl. 1): 66-71
DOI: http://dx.doi.org/10.1590/1516-1439.325514

Tensile Properties and Fracture Reliability of Melt-extracted Gd-rich Amorphous Wires

Hongxian Shen[a], Dawei Xing[a], Huan Wang[b], Jingshun Liu[c], Dongming Chen[a], Yanfen Liu[a], Jianfei Sun[a]*

[a]School of Materials Science and Engineering, Harbin Institute of Technology, Harbin 150001, China
[b]Institute for Composites Science and Innovation – InCSI, College of Materials Science and Engineering, Zhejiang University, Hangzhou 310027, China
[c]School of Materials Science and Engineering, Inner Mongolia University of Technology, Hohhot 010051, China

Received: September 9, 2014; Revised: September 30, 2015

$Gd_{60}Al_{20}Co_{20}$ amorphous wires with smooth surfaces and circular cross-sections were fabricated by a melt-extraction technique. The mechanical properties of the extracted microwires were evaluated by tensile tests and their fracture reliability was estimated by using Lognormal and two- or three- parameter Weibull analysis, respectively. The microwires exhibit a tensile fracture strength ranging from ~788 to ~1196 MPa, with a mean value of 1008 MPa and a standard variance of 121 MPa. Lognormal method of statistical analysis presents that the average stress of microwires is ~1012 MPa. Weibull statistical analysis indicates that the two-parameter tensile Weibull modulus is 8.5 and the three-parameter Weibull modulus is 5.3 with a threshold value ~365 MPa for as-extracted amorphous microwires. Our results show that the extracted Gd-based wires possess excellent tensile properties and high fracture reliability, with a high potential for applications in and magnetic refrigeration.

Keywords: *melt-extraction, metallic glass microwires, tensile property, fracture reliability*

1. Introduction

The last two decades have witnessed increasing research interest in amorphous ferromagnetic microwires. Especially, much attention has been turned to the development of potential structural and function materials with magnetic bistability[1], giant magneto impedance (GMI) effect[2-4], electromagnetic shielding (EMS)[5] by using a variety of alloy microwires. Amorphous structure for ribbons, films or BMGs are formed due to the high rapid quench rate of ~10^6 K/s which ensures the excellent mechanical[6,7] and magnetic characteristics. Melt-extracted amorphous microwires with diameters of 20~60 μm have outstanding soft magnetic characteristics[8] due to small sizes and amorphous state. The microstructure and magnetic properties of the melt-extracted microwires can be tailored by optimizing composition design or the fabrication process[9,10]. Compare with amorphous ribbons, films or bulk metallic glasses (BMGs), amorphous microwires show the superior magnetocaloric effect (MCE) due to their wire shape and fabricating process. The magnetocaloric melt-extracted microwires with a nominal composition of $Gd_{55}Al_{25}Co_{20}$ show a large magnetic entropy change ($-\Delta S_m$) of 9.7 $J \cdot kg^{-1} \cdot K^{-1}$ at 100 K[9], which is larger than that of its BMG counterpart (8.8 $J \cdot kg^{-1} \cdot K^{-1}$)[11]. The melt-extracted Gd-rich amorphous microwires have good mechanical adaptability for they are easy to be filled as different shapes, which can render them to be applied in the multifunctional fields of MCE-based refrigeration.

For improving the magnetocaloric properties and solving problems related to the practical applications of Gd-based amorphous microwires in magnetic refrigeration (MR), it is necessary to investigate their mechanical properties and fracture reliability. We have obtained a tensile fracture strength of ~1200 MPa and fracture reliability of ~800 MPa in melt-extracted $Gd_{55}Al_{25}Co_{20}$ microfibers[9], and also reported the fabrication of Zr-containing Gd-rich wires with a tensile fracture strength of ~1450 MPa and fracture reliability of ~1200 MPa[12]. So we aim to fabricate the more high-quality $Gd_{60}Al_{20}Co_{20}$ melt-extracted amorphous microwires and investigate the tensile mechanical properties and fracture reliability of these Gd-rich microwires when used as MCE materials. The fracture reliability was evaluated by using Lognormal and Weibull statistic distribution method finally.

2. Experimental Procedure

The melt-extraction technique was introduced for fabricating the microwires with a nominal composition of $Gd_{60}Al_{20}Co_{20}$. A uniform master ingot with raw materials Gd (99.5%), Al (99.99%) and Co (99.99%) was firstly fabricated by vacuum arc melting, and an alloy rod with a diameter of 10 mm was obtained by suction casting. Then the rod was placed in a boron nitride (BN) crucible and re-melted by a high frequency induction furnace. Finally, the melt was extracted by a copper wheel with a diameter of 320 mm and 60º knife-edge and the wires were formed under their surface tension and natural gravity. The constant

*e-mail: jfsun_hit@263.net, jfsun@hit.edu.cn

linear velocity of Cu wheel rim was fixed at 30 m/s and the chosen feeding rate of the molten alloy was 10-15 μm/s[13]. The melt-extracted process and the morphology of fabricated wires with high-quality are schematically shown in Figure 1. All the morphologies of wire-surface and fracture-surface after tensile test were observed on a field emission scanning electron microscope (SEM-Helios Nanolab600i) at 20 kV. The structural characteristics of the wires were identified by X-ray diffraction (XRD) test obtained by a D/max-rb with Cu Kα radiation and a differential scanning calorimeter (DSC) at a heating rate of 20 K/min. The mechanical measurements of the as-cast wires were taken on a special Instron Tensile Tester (Type: Instron-5500R1185). Special clamps were designed for wire shape samples and a mini-force sensor (the measuring range of 0~50 N) for small loading specimens were used for the tensile measurements.

3. Results and Discussions

3.1. Structural characterization

A cooling rate of ~ 10^6 K/s was achieved due to the intense heat transfer between cooling medium and liquid metal stream during fabrication process, resulting in the formation of amorphous or nanocrystalline structure of the wires. As shown in Figure 2a, a typical broad halo in XRD pattern was observed near the angle of ~ 33° and no other obvious peaks was detected, demonstrating the full amorphous nature of the wires.

As shown in Figure 2b, an obvious endothermic reaction resulting from the glass transition (super-cooled liquid region) and followed by a several obvious exothermic peaks due to crystallization appear in the DSC curve, which further indicates the amorphous feature of the micro-fibers and demonstrates a complex multi-step crystallization process. As marked with the orange and green arrows, the glass transition temperature (T_g) and starting temperature of first crystallization peak (T_{x1}) were determined as ~574 K and ~600 K respectively. The temperature region of glass transition (ΔT_x) is thus calculated as ~26 K ($\Delta T_x = T_{x1} - T_g$), displaying the glass forming ability (GFA). Both the XRD pattern and DSC curve demonstrate that the Gd-based amorphous microwires can be fabricated by melt-extraction technique.

3.2. Mechanical properties

Specimens were designed for the wire tests as shown in the inset of Figure 3a. All the strain-stress curves of measured wires are plotted in Figure 3a and it was noted that all the specimens showed brittle behavior, i.e. all the wires fail catastrophically without any plasticity. Moreover, these amorphous microwires displayed a scattering of the tensile fracture strengths (σ_F) ranging from ~788 to ~1196 MPa. In order to conveniently compare, we have re-plotted all the strain-stress curves by using the values of σ_F from the smallest to largest, as shown in Figure 3b. The average tensile fracture strength and standard deviation were statistically calculated to be ~1008 MPa and ~121 MPa respectively. The distribution of the strength-limiting flaws is considered as resulting in the strengths variation of these amorphous microwires as mentioned above, and these flaws cause the apparition of metallic cores, casting pores, inclusions or surface irregularities in the fibers which were introduced during the fabrication process. It should be noticed that the severe deterioration of mechanical properties (including tensile strength and fracture reliabilities) occurs due to the existence of these flaws, thus resulting in their limited application in MR systems.

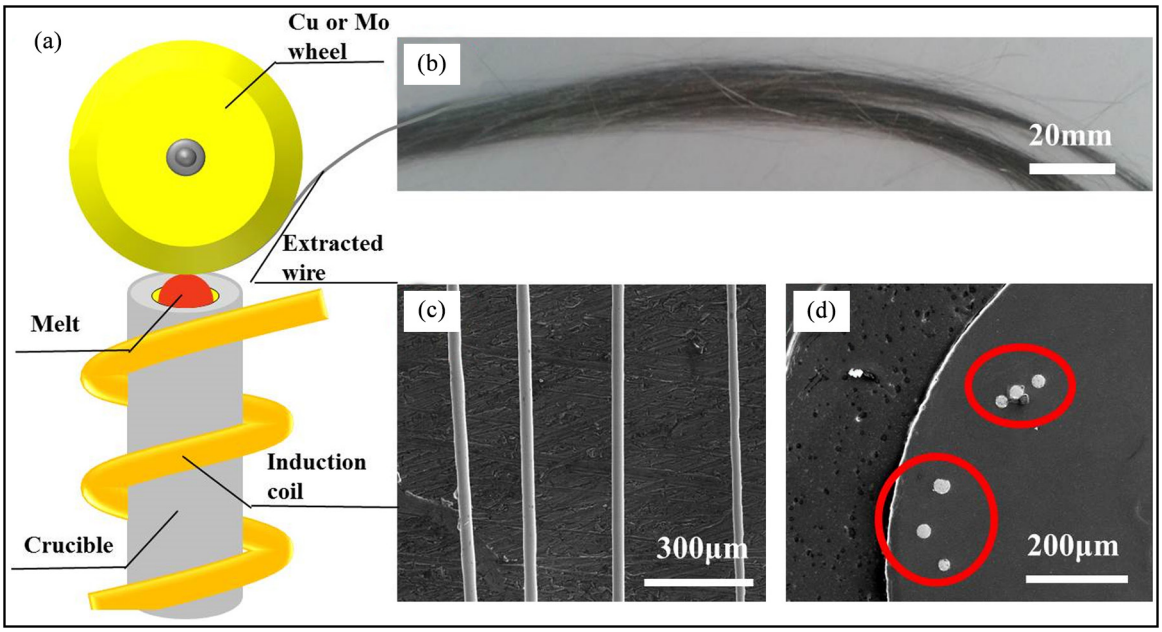

Figure 1. (a) Schematic diagram of the melt-extraction process, (b) optical micrograph of as-extracted microwires bundle, SEM images of (c) side-view and (d) circular cross-section.

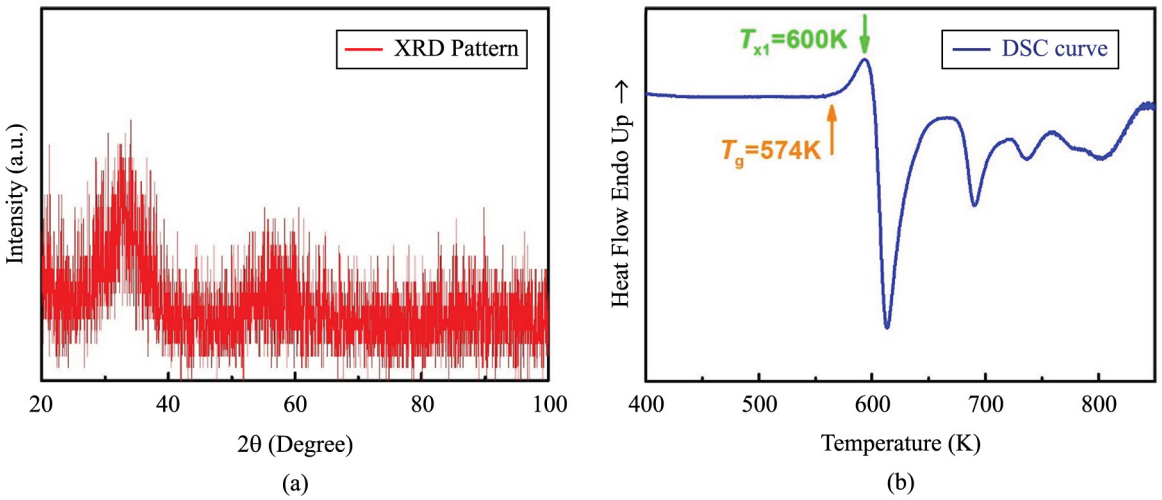

Figure 2. (a) XRD pattern and (b) differential scanning calorimeter (DSC) curve of melt-extracted $Gd_{60}Al_{20}Co_{20}$ microwires.

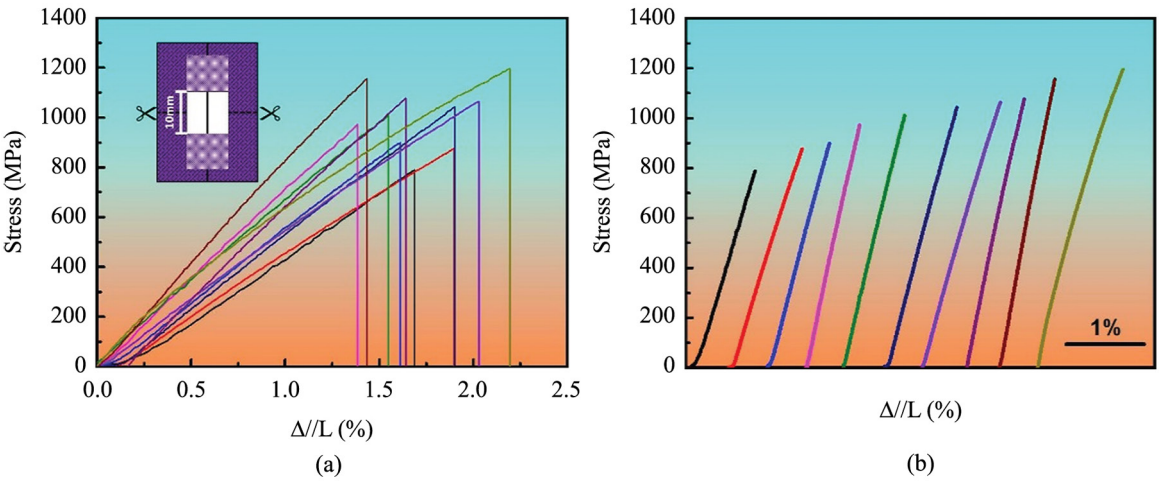

Figure 3. (a) Strain-stress curves of the tested $Gd_{60}Al_{20}Co_{20}$ microwires and inset is the wire specimen, (b) the re-plotted strain-stress curves with the values of σ_f from the smallest to largest.

The fracture reliability is vital factor in the practical applications for the brittle microwires due to their wider degree of scatter in σ_F values compared with that of ductile materials. Further to confirm the safety of brittle materials in engineering, the statistical methods are commonly employed and performed to describe the distribution of fracture stresses. Among which, Log-normal distribution method is usual for describing the failure strengths of brittle microwires and the cumulative probability function is shown as below[14]:

$$P_f^{LN} = \frac{1}{2}\left[1 + erf\left(\frac{\ln(\sigma) - \kappa}{s\sqrt{2}}\right)\right] \quad (1)$$

where P_F^{LN} shows the cumulative distribution that displays the probability of failure behavior at a given uniaxial stress σ or lower, κ is the mean and *s* represents the standard deviation of the natural log of the fracture stress values.

Further to calculate the P_F^{LN}, a set of data is obtained in Figure 3b and shown as $\sigma_1<\sigma_2<\cdots\sigma_N<\cdots<\sigma_N$. Thus the probability of failure P_I^{LN} at a uniaxial given stress σ_I can be calculated by using the following expression (median rank value):

$$P_i^{LN} = \frac{i - 0.3}{N + 0.5} \quad (2)$$

where the valus of κ and σ are obtained by fitting experimental data (ln(σ), 2 P_F^{LN} -1) which is plotted in Figure 4a and the value of R^2=0.98 shows a well-fitting result. The average stress (at κ=6.92) is calculated up to ~1012 MPa and the value is extremely close to the average stress value of ~1008 MPa.

Moreover, Weibull distribution is more commonly introduced to evaluate the brittle materials than above mentioned Log-normal distribution method and the cumulative probability function is expressed as follows[15,16]:

$$P_f^{WB} = 1 - \exp\left[-\int_V \left(\frac{\sigma - \sigma_\mu}{\sigma_0}\right)^m d_V\right] \quad (3)$$

where P_F^{WB} described Weibull cumulative distribution and defined the same as P_F^{LN}, V indicates the volume of the wire specimen, σ_μ is the threshold value of the maximum or ultimate fracture stress, σ_0 described the Weibull scale parameter (or characteristic stress) when the P_F^{WB} is 63.2% and m is the parameter known as Weibull modulus (or shape geometric parameter) which displays the variability of failure strength. While $\sigma_\mu \neq 0$, Equation 3 is rewritten by:

$$\ln\left\{\ln\left[\frac{1}{\left(1-P_f^{WB}\right)}\right]\right\} = m\ln\left(\sigma-\sigma_\mu\right) - m\ln\sigma_0 \quad (4)$$

and it also named three-parameter Weibull model (TrPWM) and when $\sigma_\mu = 0$, Equation 3 is rearranged to two-parameter Weibull model (TPWM):

$$\ln\left\{\ln\left[\frac{1}{1-P_f^{WB}}\right]\right\} = m\ln(\sigma) - m\ln(\sigma_0) \quad (5)$$

For TPWM, the values of m, σ_0 are obtained as 8.5, 1067 MPa respectively by linear fitting experimental data (ln(σ), ln[-(1-ln P_F^{WB})]) and the results show an excellent fitting for R^2=0.99. Moreover, the values of m, σ_0 and σ_μ are calculated to be 8.5, 700 MPa and 365 MPa respectively for TrPWM by non-line fitting experimental data (ln(σ), ln[-(1-ln P_F^{WB})]). The result also indicates a nearly consistent fitting of TrPWM for R^2=0.99. Though the fitting curves are quite close as shown Figure 4b, the fitting with three-parameter version (marked by violet dash line) follows the trend of the data much better than that with the two-parameter one marked by (red solid line).

It should be focused that Weibull modulus m actually described the reliability of tested specimens, namely a large value of m value represents a low degree of scatter for fracture strength and hence high reliability of applied materials. The m value calculated in our present work is larger than that of GdAlCoZr microwires[12] and A707 steel welds[17], while smaller than that of $Gd_{55}Al_{25}Co_{20}$ melt-extracted microfibers[9], Mg-based amorphous microwires[18] under tensile condition and Zr-based[19], Mg-based[20] BMGs under compressed condition. In a word, the melt-extracted $Gd_{60}Al_{20}Co_{20}$ amorphous microwires with high flaw/damage tolerance and reliability, combined with their excellent functional properties, makes them as potential substitute materials in MR applications.

3.3. Fracture morphology

Figure 5 illustrates two typical fracture morphologies observed in the tested specimens with two different diameters of ~20 μm and ~40μm. The angle between the stress axis and fracture surface varies from 52° to 82° with the diameter of the microwire increases from ~20 μm to ~40 μm, as displayed in Figures 5a and 5b. Pronounced shear bands appear in small-sized specimen, as shown in inset of Figure 5a, showing a typical fracture characteristic of amorphous alloys. The characteristic of the fracture is also reflected by the fracture morphology shown in Figure 5c which shows two pronounced regions: the relatively smooth zone (which is denoted featureless zone) induced by shear slip and the vein-pattern zone produced by the rupture of the remaining part after the initial shear displacement[21].

In comparison, Figure 5d shows the clear cross-section of a perpendicular fracture for the relatively larger diameter specimen, which is similar to the low-strength fracture surface of Mg-based wires. The crack originated at one of the surface irregularities formed during the fabricated process, and moved radially away from a semicircular ‘‘mirror”, leaving elongated markings along the crack propagation paths to form ‘‘hackle regions”, and finally resulted in the fracture of the wire. This larruping fracture morphology and relatively large angle between the stress axis and fracture surface caused by a low amorphization degree owing to the lower solidification rate during fabrication process with large diameters. However, there is almost no obvious tensile plasticity detected in all tested samples, nearly indicating their brittle nature.

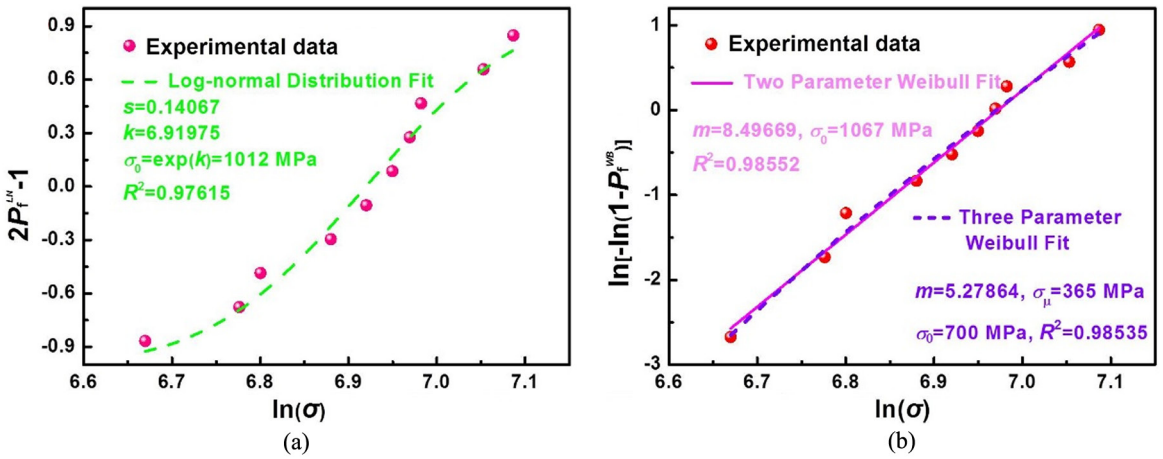

Figure 4. (a) Log-normal poltting and (b) Weibull plotting of the tensile strength of amorphous melt-extracted $Gd_{60}Al_{20}Co_{20}$ microwires

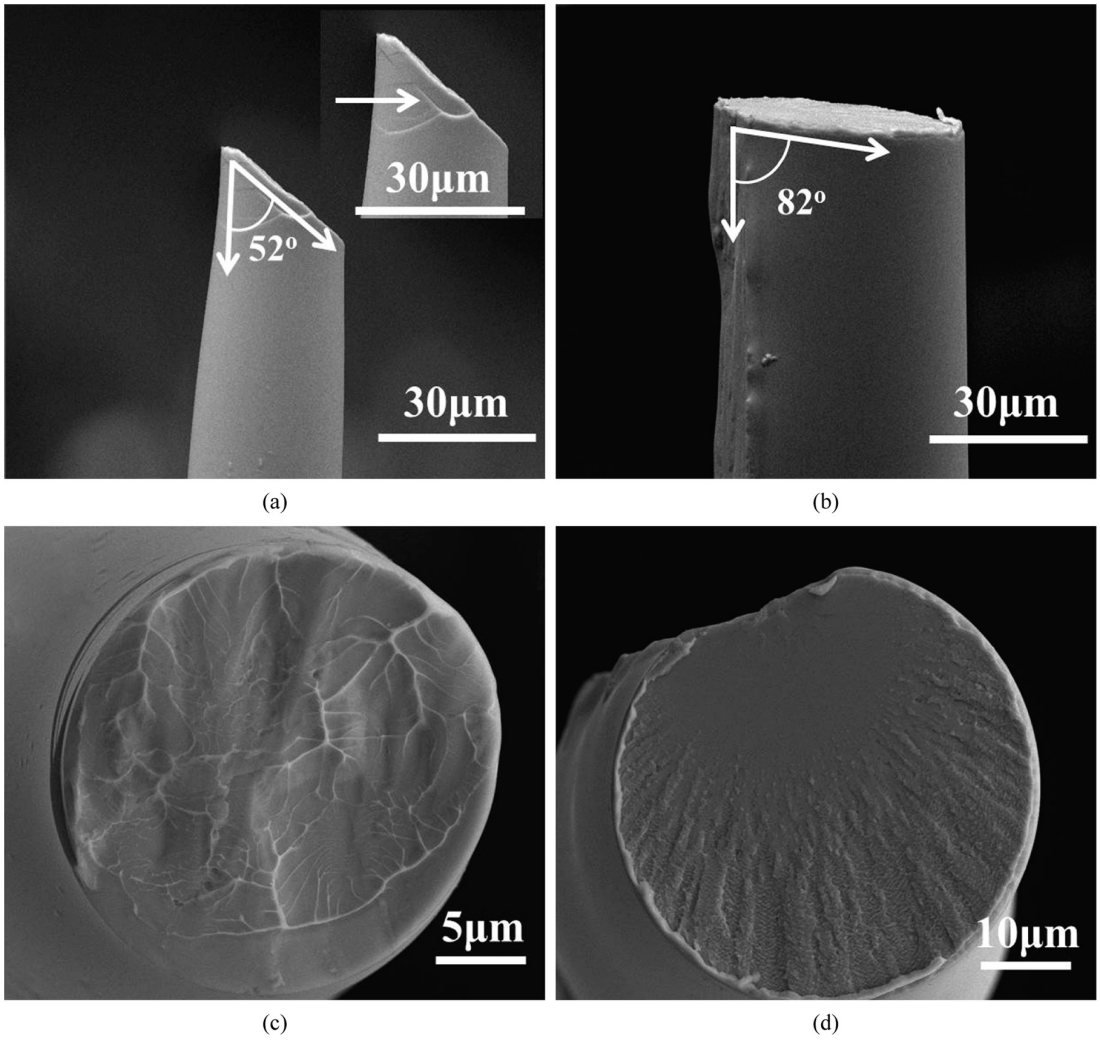

Figure 5. Fracture morphologies of melt-extracted $Gd_{60}Al_{20}Co_{20}$ amorphous microwires with diameters of (a) ~20μm (the inset gives the local magnified image of (a)) and (b) ~40 μm for side-view. (c) and (d) show the cross-section images of (a) and (b).

4. Conclusions

The mechanical properties and fracture reliability of melt-extracted $Gd_{60}Al_{20}Co_{20}$ amorphous microwires were systematically investigated. The tensile fracture strengths of tested wires vary from ~788 to ~1196 MPa, and their mean values and standard deviation were calculated to be ~1000 MPa and 121 MPa, respectively. The wires exhibited a brittle fracture characteristic and the average stress of 1012 MPa is obtained by Log-normal fitting. The larger values of Weibull modulus of 8.5 and 5.3 calculated by two-parameter or three-parameter Weibull non-line fitting method respectively, pronounced high flaw/damage tolerance and reliability of the melt-extracted Gd-based amorphous wires. Therefore, the more excellent tensile property and higher fracture reliability together with their excellent previously reported magnetocaloric property of the Gd-based wires make them potential materials for magnetic refrigeration applications.

Acknowledgements

This work was financially supported by National Natural Science Foundation of China (NSFC) under grant Nos. 51371067. J.S. Liu acknowledges the financial support provided by the National Natural Science Foundation of China (NSFC) under grant Nos. 51401111 and 51561026, Natural Science Foundation of Inner Mongolia Autonomous Region of China under grant Nos. 2014BS0503.

References

1. Qin FX and Peng HX. Ferromagnetic microwires enabled multifunctional composite materials. *Progress in Materials Science*. 2013; 58(2):183-259. http://dx.doi.org/10.1016/j.pmatsci.2012.06.001.

2. Liu JS, Qin FX, Chen DM, Shen HX, Wang H, Xing DW, et al. Combined current-modulation annealing induced enhancement of giant magnetoimpedance effect of co-rich amorphous microwires. *Journal of Applied Physics*. 2014; 115(17):17A326. http://dx.doi.org/10.1063/1.4865460.

3. Wang H, Qin FX, Xing DW, Cao FY, Peng HX and Sun JF. Fabrication and characterization of nano/amorphous dual-phase finemet microwires. *Materials Science and Engineering B*. 2013; 178(20):1483-1490. http://dx.doi.org/10.1016/j.mseb.2013.09.010.
4. Chen DM, Xing DW, Qin FX, Liu JS, Wang H, Wang XD, et al. Correlation of magnetic domains, microstructure and gmi effect of joule-annealed melt-extracted $Co_{68.15}Fe_{4.35}Si_{12.25}B_{13.75}Nb_1Cu_{0.5}$ microwires for double functional sensors. *Physica Status Solidi A: Applications and Materials Science*. 2013; 210(11):2515-2520. http://dx.doi.org/10.1002/pssa.201329246.
5. Zhang Z, Wang C, Zhang Y and Xie J. Microwave absorbing properties of composites filled with glass-coated $Fe_{69}Co10Si_8B_{13}$ amorphous microwire. *Materials Science and Engineering B*. 2010; 175(3):233-237. http://dx.doi.org/10.1016/j.mseb.2010.07.034.
6. Wang H, Qin FX, Xing DW, Cao FY, Wang XD, Peng HX, et al. Relating residual stress and microstructure to mechanical and giant magneto-impedance properties in cold-drawn co-based amorphous microwires. *Acta Materialia*. 2012; 60(15):5425-5436. http://dx.doi.org/10.1016/j.actamat.2012.06.047.
7. Liao WB, Zhao YY, He JP and Zhang Y. Tensile deformation behaviors and damping properties of small-sized Cu-Zr-Al metallic glasses. *Journal of Alloys and Compounds*. 2013; 555:357-361. http://dx.doi.org/10.1016/j.jallcom.2012.12.110.
8. Liu JS, Cao FY, Xing DW, Zhang LY, Qin FX, Peng HX, et al. Enhancing GMI properties of melt-extracted co-based amorphous wires by twin-zone joule annealing. *Journal of Alloys and Compounds*. 2012; 541:215-221. http://dx.doi.org/10.1016/j.jallcom.2012.05.126.
9. Shen HX, Wang H, Liu JS, Xing DW, Qin FX, Cao FY, et al. Enhanced magnetocaloric and mechanical properties of melt-extracted $Gd_{55}Al_{25}Co_{20}$ micro-fibers. *Journal of Alloys and Compounds*. 2014; 603:167-171. http://dx.doi.org/10.1016/j.jallcom.2014.03.053.
10. Bingham NS, Wang H, Qin FX, Peng HX, Sun JF, Franco V, et al. Excellent magnetocaloric properties of melt-extracted Gd-based amorphous microwires. *Applied Physics Letters*. 2012; 101(10):102407. http://dx.doi.org/10.1063/1.4751038.
11. Du J, Zheng Q, Li YB, Zhang Q, Li D and Zhang ZD. Large magnetocaloric effect and enhanced magnetic refrigeration in ternary gd-based bulk metallic glasses. *Journal of Applied Physics*. 2008; 103(2):023918. http://dx.doi.org/10.1063/1.2836956.
12. Qin FX, Bingham NS, Wang H, Peng HX, Sun JF, Franco V, et al. Mechanical and magnetocaloric properties of gd-based amorphous microwires fabricated by melt-extraction. *Acta Materialia*. 2013; 61(4):1284-1293. http://dx.doi.org/10.1016/j.actamat.2012.11.006.
13. Wang H, Xing DW, Wang XD and Sun JF. Fabrication and characterization of melt-extracted co-based amorphous wires. *Metallurgical and Materials Transactions A: Physical Metallurgy and Materials Science*. 2010; 42(4):1103-1108. http://dx.doi.org/10.1007/s11661-010-0459-0.
14. Sharpe WN Jr, Pulskamp J, Gianola DS, Eberl C, Polcawich RG and Thompson RJ. Strain measurements of silicon dioxide microspecimens by digital imaging processing. *Experimental Mechanics*. 2007; 47(5):649-658. http://dx.doi.org/10.1007/s11340-006-9010-z.
15. Weibull W. A statistical distribution function of wide applicability. *Journal of Applied Mechanics*. 1951; 18(3):293-297.
16. Han Z, Tang LC, Xu J and Li Y. A three-parameter weibull statistical analysis of the strength variation of bulk metallic glasses. *Scripta Materialia*. 2009; 61(9):923-926. http://dx.doi.org/10.1016/j.scriptamat.2009.07.038.
17. Zhou J and Soboyejo W. A statistical approach to the prediction of brittle fracture in heat-affected zones of A707 steel welds. *Materials and Manufacturing Processes*. 2004; 19(5):921-947. http://dx.doi.org/10.1081/AMP-200030653.
18. Zberg B, Arata ER, Uggowitzer PJ and Löffler JF. Tensile properties of glassy mgznca wires and reliability analysis using weibull statistics. *Acta Materialia*. 2009; 57(11):3223-3231. http://dx.doi.org/10.1016/j.actamat.2009.03.028.
19. Gao HL, Shen Y and Xu J. Weibull analysis of fracture strength for $Zr_{55}Ti_2Co_{28}Al_{15}$ bulk metallic glass: tension-compression asymmetry and porosity effect. *Journal of Materials Research*. 2011; 26(16):2087-2097. http://dx.doi.org/10.1557/jmr.2011.210.
20. Zhao YY, Ma E and Xu J. Reliability of compressive fracture strength of Mg-Zn-Ca Bulk metallic glasses: flaw sensitivity and weibull statistics. *Scripta Materialia*. 2008; 58(6):496-499. http://dx.doi.org/10.1016/j.scriptamat.2007.10.052.
21. Wang H, Xing DW, Peng HX, Qin FX, Cao FY, Wang GQ, et al. Nanocrystallization enabled tensile ductility of co-based amorphous microwires. *Scripta Materialia*. 2012; 66(12):1041-1044. http://dx.doi.org/10.1016/j.scriptamat.2012.02.020.